Stem Cell Reports
Report
OPEN ACCESS

FGF2 Induces Migration of Human Bone Marrow Stromal Cells by Increasing Core Fucosylations on N-Glycans of Integrins

Baarkullah Awan,[1,6] David Turkov,[1,6] Cameron Schumacher,[1] Antonio Jacobo,[1] Amber McEnerney,[1] Ashley Ramsey,[1] Gege Xu,[2] Dayoung Park,[2] Stefanos Kalomoiris,[1] Wei Yao,[3] Li-En Jao,[4] Miguel L. Allende,[4,5] Carlito B. Lebrilla,[2] and Fernando A. Fierro[1,4,*]

[1]Institute for Regenerative Cures, University of California, Davis, Sacramento, CA, USA
[2]Department of Chemistry, University of California, Davis, Davis, CA, USA
[3]Center for Musculoskeletal Health, Department of Internal Medicine, University of California, Davis, Davis, CA, USA
[4]Department of Cell Biology and Human Anatomy, University of California, Davis, Davis, CA, USA
[5]Center for Genome Regulation, Facultad de Ciencias, Universidad de Chile, Santiago, Chile
[6]Co-first author
*Correspondence: ffierro@ucdavis.edu
https://doi.org/10.1016/j.stemcr.2018.06.007

SUMMARY

Since hundreds of clinical trials are investigating the use of multipotent stromal cells (MSCs) for therapeutic purposes, effective delivery of the cells to target tissues is critical. We have found an unexplored mechanism, by which basic fibroblast growth factor (FGF2) induces expression of fucosyltransferase 8 (FUT8) to increase core fucosylations of N-linked glycans of membrane-associated proteins, including several integrin subunits. Gain- and loss-of-function experiments show that FUT8 is both necessary and sufficient to induce migration of MSCs. Silencing FUT8 also affects migration of MSCs in zebrafish embryos and a murine bone fracture model. Finally, we use *in silico* modeling to show that core fucosylations restrict the degrees of freedom of glycans on the integrin's surface, hence stabilizing glycans on a specific position. Altogether, we show a mechanism whereby FGF2 promotes migration of MSCs by modifying N-glycans. This work may help improve delivery of MSCs in therapeutic settings.

INTRODUCTION

Despite the marked safety profile and long-established potential of multipotent stromal cells (MSCs) to promote tissue repair, their use has been limited mostly to small clinical trials, with only modest efficacy (Trounson and McDonald, 2015). A major barrier to the effective application of MSCs has been the poor ability to target these cells to tissues of interest (Karp and Leng Teo, 2009). For example, therapies aiming for bone repair require that injected cells home to the bone marrow, a process that is highly inefficient (Grayson et al., 2015; Rombouts and Ploemacher, 2003).

Glycosylation is a common post-translational modification of proteins that affects many cell functions, including adhesion, migration, and signaling (Cummings and Pierce, 2014; Moremen et al., 2012). N-glycans are sugars attached to Asparagine in Asn-X-Ser/Thr peptides, where X can be any amino acid, except for proline. It has been proposed that N-linked glycosylations (N-glycans) may affect cell migration both positively and negatively (Gu and Taniguchi, 2008), although the experimental evidence is mostly limited to selectin binding. Of note, chemical engineering of glycosylations promotes MSC homing to the bone marrow (Sackstein et al., 2008), suggesting that N-glycans could play a critical role in MSC migration.

During MSC expansion, basic fibroblast growth factor (FGF2) is often used to increase cell proliferation (Tsutsumi et al., 2001), maintain differentiation potential (Solchaga et al., 2005), and delay cellular senescence (Ito et al., 2007). It has also been shown that FGF2 promotes migration of MSCs *in vitro* (Schmidt et al., 2006), although no potential mechanism for FGF2-mediated migration has been described. Therefore, we aimed to determine changes at mRNA and N-glycan levels that could account for increased migration of MSCs, potentially leading to new approaches to improve MSC delivery.

RESULTS

FGF2 Promotes Migration of MSCs by Altering Gene Expression and N-Glycans

To test the effect of FGF2 on migration of MSCs, two experimental approaches were used. In the wound/scratch assay, MSCs are seeded so that a constant gap or "wound" is left in-between the monolayer of cells. Closure of the wound over time is therefore proportional to the migration ability of the cells. To complement this assay, we used single-cell tracking, where the displacement of individual cells over time (speed) is recorded using videomicroscopy. In both *in vitro* assays, treatment with FGF2 significantly increased migration of MSCs (Figures 1A, 1B, and S1).

To identify changes in gene expression that could account for increased migration, we performed deep-sequencing transcriptome analysis (RNA-seq) on MSCs

This is an open access article under the CC BY-NC-ND license (http://creativecommons.org/licenses/by-nc-nd/4.0/).

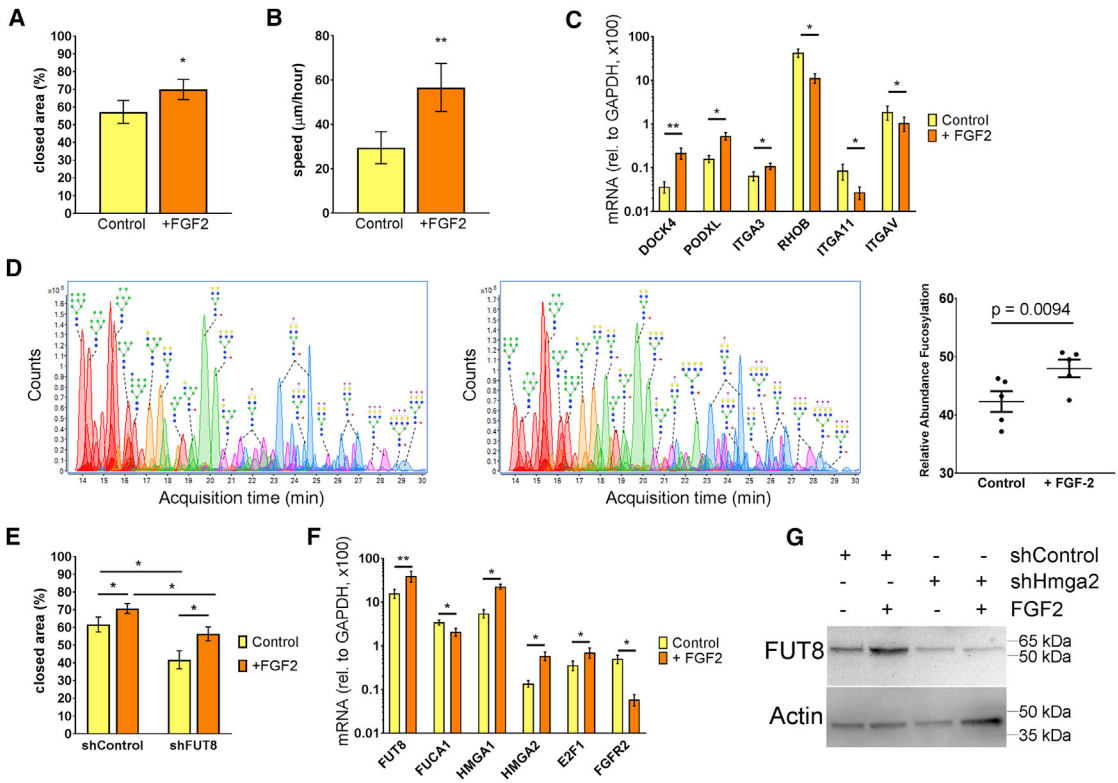

Figure 1. FGF2 Promotes Migration by Increasing FUT8 and Core Fucosylations

(A) Wound/scratch assay, where closed area represents MSC migration after 24 hr, N = 5.

(B) Cell tracking using videomicroscopy. MSC displacement over time (speed) was recorded for 24 hr and tracked using ImageJ software. A total of 30 cells per condition (derived from two different donors) were analyzed.

(C) RT-PCR confirming differential expression of genes related to cell migration, N = 6.

(D) Representative chromatograms of N-glycans detected by MS and semi-quantification of core-fucosylation levels, N = 5.

(E) Wound/scratch assay showing the effect of silencing FUT8 on FGF2-induced migration (N = 6).

(F) RT-PCR showing differential expression of genes associated with core fucosylations and FUT8 expression, N = 6.

(G) Western blots in MSCs transduced with the indicated lentivirus and treated with or without FGF2 (N = 3).

Error bars indicate standard error of the mean (SEM). For all statistical analyses, a paired Student's t test was used, where *$p < 0.05$ and **$p < 0.005$, and N indicates biological replicates (MSCs derived from different donors).

cultured with or without FGF2 (Figure S2 and GEO repository). A large-scale gene function analysis of the 246 transcripts increased with FGF2 revealed a strong enrichment for genes related to cell-cycle progression and proliferation (Figure S2). Among the 267 downregulated transcripts, collagen-related processes were highly represented. We also confirmed several migration-related genes as regulated by FGF2, including upregulation of *DOCK4*, *PODXL*, and *ITGA3* and downregulation of *RHOB*, *ITGA11*, and *ITGAV* (Figure 1C). These results suggest that FGF2 promotes migration of MSCs through coordinated regulation of multiple genes.

We next investigated if FGF2 could also induce post-translational changes that could account for increased migration. A major modification in membrane-associated proteins (MAPs) are N-glycans that occur in the ER and Golgi apparatus. In fact, we found multiple glycosylation-related genes differentially expressed with FGF2 (Figure S2B). Therefore, MSCs were treated with or without FGF2 and processed for extraction of MAPs and semi-quantitative analysis by mass spectrometry (MS) (Park et al., 2015). We found a decrease in high-mannose N-glycans and a mild trend to increase sialylations (Figure S1), whereas the most consistent observation was an increase in fucosylated N-glycans (Figure 1D). Most fucosylated N-glycans (92.7%) showed one fucose, which is usually attached to the first N-acetylglucosamine within the chitobiose core and are therefore called core fucosylation.

Notably, the MS analysis was in accordance with the RNA-seq data, because core fucosylations are catalyzed by α-1,6-fucosyltransferase (FUT8) (Yang and Wang, 2016), and FUT8 was significantly upregulated by

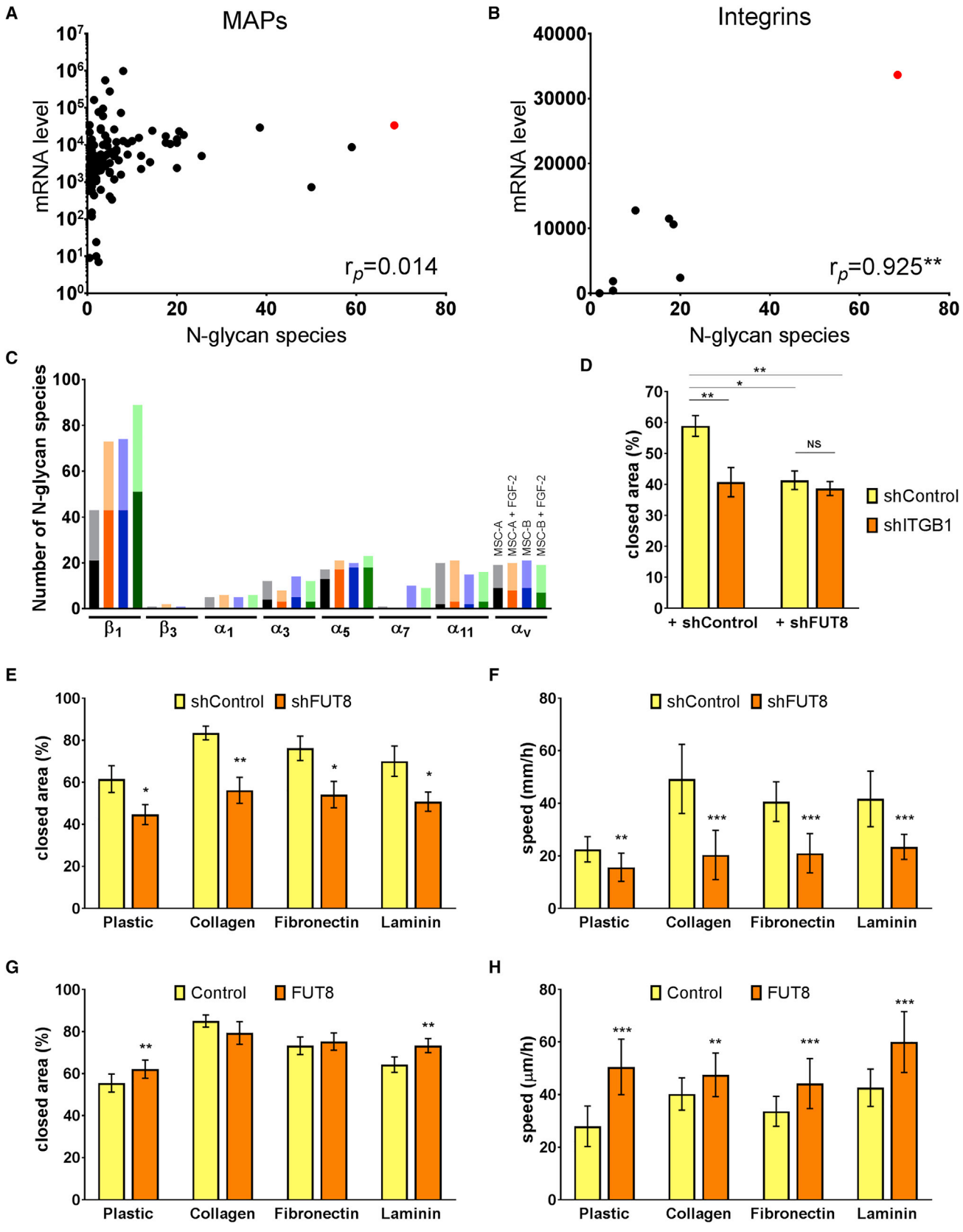

(legend on next page)

FGF2 (Figure 1F). Hydrolysis of core fucosylations is catalyzed by both α-L-fucosidase 1 (*FUCA1*) and *FUCA2*. Expression of *FUCA2* was not affected by FGF2, while FUCA1 was downregulated by FGF2, although this reduction (0.2-fold) was not as pronounced as the increase in FUT8 (2.0-fold). Since fibroblasts derived from FUT8$^{-/-}$ mice show impaired migration (Zhao et al., 2006), we tested if FUT8 would affect migration of human MSCs. Indeed, the increased migration induced by FGF2 was strongly reduced in MSCs transduced with a lentivirus to silence FUT8 (shFUT8; Figure 1E), suggesting that core fucosylations are necessary for migration of MSCs.

We previously showed that FGF2 quickly increases High-Mobility Group 2A (*HMGA2*) mRNA and protein levels in MSCs (Kalomoiris et al., 2016). In addition to HMGA2, we also found the homolog *HMGA1* strongly increased by FGF2 (Figure 1F). To test if the increase of FUT8 is regulated by *HMGA2*, we transduced MSCs with either a control short hairpin RNA (shControl) or a shRNA to silence *HMGA2* (shHMGA2) and then incubated the cells with or without FGF2. In MSCs transduced with shControl, FGF2 markedly increased FUT8 protein expression. However, in MSCs transduced with shHMGA2, FUT8 expression was very low, even in the presence of FGF2, suggesting that HMGA2 acts downstream of FGF2 to regulate FUT8 expression (Figure 1G). To determine potential transcription factors that could induce FUT8 expression, we found that the FUT8 promoter shows multiple E2F binding sites, including at least three for E2F1. Interestingly, *E2F1* expression was increased with FGF2 (Figure 1F), while others have shown that HMGA2 increases E2F1 activity (Fedele et al., 2006). Overall, these results suggest that FGF2 increases core fucosylations through a signaling pathway involving HMGA2, leading to transcriptional increase of FUT8.

Fucosylation of Integrins Are Essential for Migration of MSCs

To determine which specific MAPs were core-fucosylated, we used a liquid chromatography-tandem MS (LC-MS/MS)-based multiple reaction monitoring (MRM) approach for glycoprotein analysis (Hong et al., 2013). We consistently detected a total of 241 peptides corresponding to 118 different MAPs, treated with or without FGF2 (Table S1). Most proteins showed 1–10 different types of N-glycans (average 6.5; Figure 2A) and no correlation was found between relative mRNA levels (determined by RNA-seq) and number of types of N-glycans (measured by MRM). However, among integrins, mRNA levels strongly correlated with the variety of N-glycans found (Figure 2B). Integrin β_1 stands out for exhibiting on average 70 different types of N-glycans, 56% of them fucosylated. Also, integrin subunits α_3, α_5, α_{11}, and α_V showed fucosylated N-glycans, although at low levels, as compared with β_1 (Figure 2C). These results show that various integrins, and especially subunit β_1, are core-fucosylated.

The role of core fucosylation on integrin β_1 was experimentally supported by a wound/scratch assay. Here, silencing FUT8 shows the same inhibitory effect as silencing integrin β_1, while silencing both FUT8 and integrin β_1, leads to no additional inhibition (Figure 2D).

To further assess the functional effect of core fucosylations, we performed migration assays over different extracellular matrix, known to be specific integrin ligands. Based on integrin's expression levels and fucosylations, we used collagen I to assess $\alpha_{11}\beta_1$, fibronectin to assess $\alpha_5\beta_1$ and $\alpha_V\beta_1$, and laminin to assess for $\alpha_3\beta_1$ activity. Using the wound/scratch assay and single-cell tracking, we found that silencing FUT8 inhibited migration on all substrates (Figures 2D and 2E). In the wound/scratch assay, over-expression of FUT8 increased MSC migration over polystyrene (uncoated plates) and laminin (Figure 2F), while over collagen and fibronectin, MSCs virtually closed the wounds within 24 hr, hence no additional increase in migration could be detected. However, in single-cell tracking assays, over-expression of FUT8 increased migration of MSCs on all surfaces tested (Figure 2G). These results suggest that core fucosylations

Figure 2. Core Fucosylations on Integrins Regulate Migration of MSCs

(A) Correlation analysis of membrane associated proteins mRNA (as determined by RNA-seq; N = 4) and number of N-glycans types found by MRM/MS (N = 2, each with and without FGF2). Integrin β_1 is highlighted in red.

(B) Correlation analysis of integrins, **p = 0.0011, as determined using a Pearson correlation analysis.

(C) Number of N-glycans found in integrins expressed in MSCs. Dark section of each column denotes fucosylated N-glycans, light section is non-fucosylated N-glycans.

(D) Wound/scratch assay on uncoated plates of MSCs transduced twice, with either shControl or shITGB1 (to silence integrin β_1), and shControl or shFUT8. N = 6.

(E and G) Wound/scratch assays of MSCs cultured over different substrates; N = 6 for both experiments.

(F and H) Videomicroscopy over 12 hr of MSCs cultured over different substrates, transduced to either silence (E) or over-express (G) FUT8. N = 30 cells, derived from three different donors.

Error bars indicate standard error of the mean (SEM). Statistical differences were determined using two-way ANOVA with post hoc Student's t test (paired for D, E, and G and non-paired for F and H), where *p < 0.05 and **p < 0.005. ***p < 10^{-5}, and N indicates biological replicates, except when otherwise indicated.

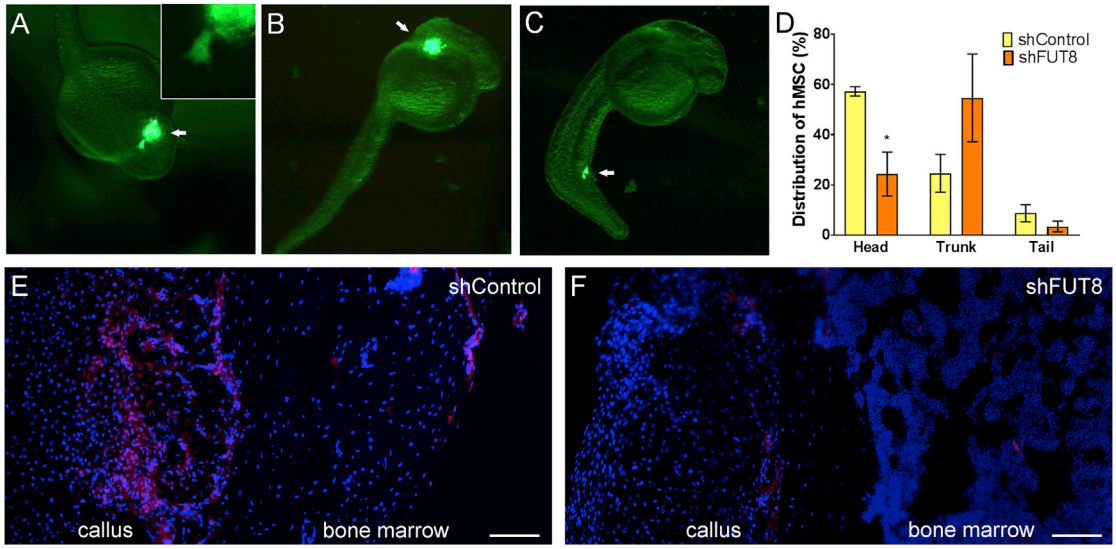

Figure 3. Silencing FUT8 Affects Migration of MSC in Zebrafish and Mice

(A) Representative image of GFP-expressing human MSCs around the head of 1-dpf zebrafish. Insert shows high magnification, where protrusions from an individual cell are visible.

(B) MSCs distributed around the trunk region.

(C) MSCs distributed in the tail. Distribution of transplanted cells is highlighted by arrows.

(D) Quantification of cell distribution, where *$p < 0.05$ as assessed using a paired Student's t test ($N = 5$ independent experiments performed with biological replicates).

(E) Seven days after bone fracture and intramuscular injection of cells, mice were analyzed for presence of tdTomato-expressing mouse MSCs. Control cells distribute abundantly in callus and bone marrow of the fractured femur.

(F) MSCs with shFUT8 only minimally reach the new callus and bone marrow on fracture site.

Error bars indicate standard error of the mean (SEM). Scale bars, 100 μm.

on integrin β_1 are both necessary and sufficient to promote MSC migration.

FUT8 Is Necessary for Migration of MSCs *In Vivo*

Zebrafish embryos have been used as platforms for assaying mammalian cancer cell behavior, as xenotransplanted cells develop tumors and metastasize (Marques et al., 2009). The transparency of embryos and absence of a functional innate immune system until 2 days post fertilization (dpf), allow imaging of fluorescently labeled transplanted cells over time. To study the role of FUT8 on migration of MSCs *in vivo*, we introduced green or red fluorescently labeled MSCs into wild-type zebrafish blastulae (4 hr postfertilization [hpf]). One day after transplantation, control MSCs distributed mostly in the anterior embryo (brain, eye, heart, gill arches) and, to a lesser extent, in the trunk and tail (Figures 3A and 3B). In contrast, shFUT8 transduced MSCs accumulate almost exclusively in the lateral trunk, often directly under the skin (posterior to the hindbrain and anterior to the yolk extension; Figure 3C), and they tended to clump together. We quantified the position of MSCs along the anterior-posterior axis and found a significant difference between control and FUT8 mRNA-depleted cells (Figure 3D).

We recently showed that over-expression of FGF2 in MSCs accelerates bone repair in mice, which we hypothesized is driven by increased migration, since with FGF2, more MSCs were found at the fracture site at early time points (Zhang et al., 2017). We therefore tested if inhibition of FUT8 would alter the incorporation of MSCs into the fractured femur. Immediately following a femoral fracture in the right hindlimb, FGF2-treated cells (transduced with either shControl or shFUT8) were injected into both left and right thighs close to the fracture site. Cells were then allowed to migrate toward the fracture site for 7 days. As previously reported (Zhang et al., 2017), only a very few cells incorporated into the left, unfractured, femur (not shown). On the fractured site, control MSCs were abundantly found incorporated into the callus and some cells were observed in the bone marrow. In contrast, MSCs transduced with shFUT8 were barely detectable at the fracture site. Since these cells were still present in the muscle (around the injection site), we conclude that shFUT8 did not affect cell retention, but rather inhibited cell migration toward the fracture site. These results further support that FUT8 is essential for migration of MSCs *in vivo*.

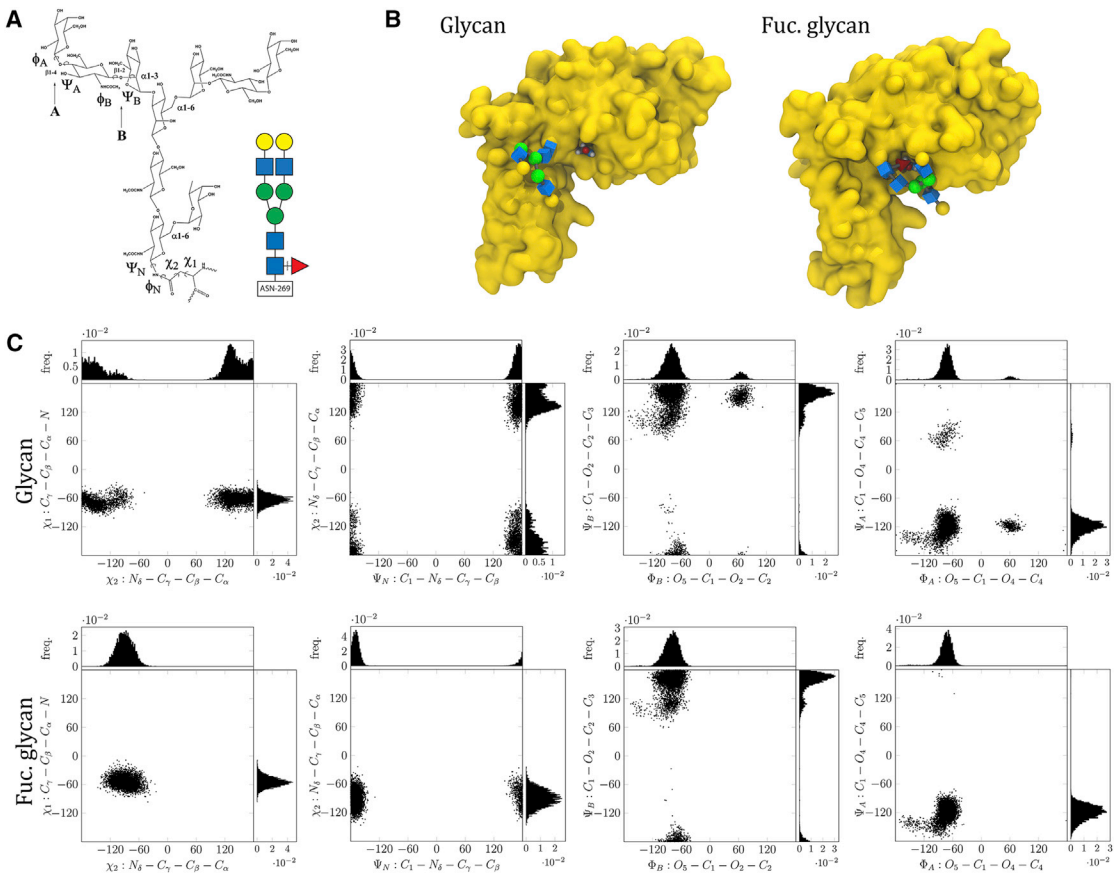

Figure 4. Molecular Modeling Suggests that Core Fucosylations Alter the Orientation of N-Glycans on Integrin β_1

(A) Schematic view of N-glycan analyzed, depicting dihedral angles; colored insert shows a cartoon version, where blue squares are N-acetylglucosamine, green circles are mannose, yellow circles are galactose, and red triangle is fucose.

(B) Extracellular domain of integrin β_1 with N-glycan and fucosylated N-glycan. Amino acid Asp_{329} is highlighted; during modeling, the fucosylated N-glycan often establishes hydrogen bonds with it.

(C) Torsion dihedral angles over simulation showing more restricted N-glycan orientation with core fucosylation.

Core Fucosylation May Limit the Movement of N-Glycans

To study how core fucosylations affect protein function, we used molecular dynamics. We detected six glycosylated residues on integrin β_1, all in the extracellular domain, facing the surface of the protein (Video S1). We performed minimization and equilibration calculations to attach *in silico* one glycan (Figure 4A) to Asn_{265} as actually found in our MRM analysis in both forms, with and without core fucose. After extensive equilibration, we performed simulations and found that the fucosylated glycan shows more restricted movement, as compared with the non-fucosylated glycan (Videos S2 and S3). This was at least partially due to hydrogen bonds built in-between the fucose and Asn_{329} (Figure 4B). The restricted movements of the fucosylated glycan were also noticeable in dihedral angles. Interestingly, we found the strongest effects on the bond in-between the glycan and Asn_{265} (torsions of the acetamido and hydroxymethyl groups) and on the α1,3 antenna (torsion angles A and B) (Figure 4C). In contrast, dihedral angles along the center portion (chitobiose core) of the glycan and the α1,6 antenna were only minimally altered (Figure S4). Altogether, molecular dynamics suggest that core fucosylations may reduce total glycan ensembles, possibly favoring the interaction of the glycan with other molecules.

DISCUSSION

Our gain- and loss-of function experiments demonstrate that FUT8 affects migration of MSCs. Core fucosylations on N-glycans attached to integrin β_1 seemed particularly relevant, because integrin β_1 showed over ten times more types of N-glycans as compared with the average for MAPs. Also, silencing integrin β_1 or FUT8 inhibited

migration similarly, with no additive effect when silencing both genes together. Of note, in fibroblasts, regulation of integrins is associated with the different α subunits, while β_1 integrin is considered to be synthesized in excess (Heino et al., 1989). We now propose that β_1 integrin is primarily regulated at the post-translational level. Integrin β_1 is the predominant adhesion receptor subfamily in human MSCs (Gronthos et al., 2001), where ligand binding, dimerization, or clustering (Guo et al., 2002) and interaction with tetraspanins (Goschnick et al., 2006) are all likely dependent on changes on glycosylation.

Our study in mice with bone fracture further supports a critical role of FUT8 on cell migration, but how reduced migration affects the therapeutic effect of MSCs remains unknown. Bone repair is assessed 3–8 weeks after fracture, while we determined incorporation of cells into the fracture 1 week after injection. Also, future work is necessary to determine if pre-incubation with FGF2 or direct increase of core fucosylations on integrin β_1 can improve MSC homing.

Xenotransplantation of human MSCs in zebrafish is a promising tool to assess cell migration *in vivo*, even at the single-cell level. Future work is necessary to understand how in this model, cell migration is dictated, since it possibly involves chemotaxis, adhesion, and cell motility.

Since core fucosylations associate with various types of metastatic tumors (Geng et al., 2004; Taniguchi and Kizuka, 2015; Wang et al., 2014), it will be important to determine if our findings are confirmed in other cell types, including cancer cells.

In accordance with the mitogenic effect of FGF2 on MSCs, we found that most of the upregulated genes with FGF2 relate to cell-cycle progression and proliferation. Arguably, the wound/scratch assays with FGF2 could be biased by increased cell numbers. However, after 24 hr, MSCs treated with FGF2 are only 10% more than control cells (not shown), indicating that most of the wound closure is due to an effect on cell migration, rather than proliferation. Similarly, we observed that immediately after cell division, MSCs exert the highest motility. We therefore avoided tracking cells that had undergone recent (within 1 hr) cell division. Of note, FGF2 reduces cell adhesion to uncoated plates, a process that was not affected by either silencing or over-expressing FUT8 (not shown).

Many genes are regulated by both HMGA1 and HMGA2, but some genes are specifically regulated by only one of them (Federico et al., 2014). Since HMGA2 strongly increases E2F1 activity (Fedele et al., 2006), but we found both HMGA1 and HMGA2 increased by FGF2, it will be important to test if also silencing HMGA1 could affect FGF2 -mediated FUT8 expression. It will be also relevant to verify the FGF2/HMGA2/FUT8 pathway in other types of stem cells, because in many of them HMGA2 is an essential regulator of self-renewal.

In addition to increased core fucosylations with FGF2, we also found a decrease in high-mannose N-glycans. This is consistent with the notion that high-mannose N-glycans need to be first trimmed in the ER membrane, prior to being core-fucosylated in the late Golgi cisternae (Kornfeld and Kornfeld, 1985). The role of most N-glycan modifications in MSCs remains unknown and deserves future investigation. In addition to migration, N-glycans may affect receptor function or the interaction with other cells and substrates.

Finally, altering integrin function affects migration, but also adhesion and survival, and can even define cell fate under differentiation cues (Dalby et al., 2014). Although technically challenging, changes in N-glycans of specific proteins or even specific residues hold the potential to modulate and alter protein function. Our results suggest that FGF2 triggers transcriptional changes, which lead to post-translational modifications, hence affecting cellular migration in a highly complex, but coordinated way.

EXPERIMENTAL PROCEDURES

Cell Culture

Human and mouse MSCs were isolated from bone marrow (Fierro et al., 2011). Each experiment repetition (N) was performed with MSCs derived from a different donor. All experiments with FGF2 use 24-hr incubation, 10 ng/mL FGF2.

In Vitro Migration Assays

For the wound/scratch assay, MSCs were seeded into plates with Cytoselect inserts. The next day, inserts were removed, leaving a "wound" (open area), and pictures were taken immediately and 24 hr after, unless otherwise described. For videomicroscopy, cell displacement was recorded using in a BioStation microscope.

RNA-Seq

Total RNA from four different donors treated with or without FGF2 sequencing was performed in two SE50 lanes using the Hiseq2000 platform (Illumina).

Mass Spectrometry

For N-glycan analysis, cells were processed for NanoLC/ESI-QTOF-MS, as previously described (Park et al., 2015). For LC-MS/MS analysis, enriched glycopeptides were identified using a Q Exactive Plus mass spectrometer.

Migration Assay toward Bone Fracture in Mice

Studies in mice were performed strictly following protocols approved by the Institutional Animal Care and Use Committee (IACUC) at UC Davis. Closed transverse diaphysis fractures of the right femur were generated as previously described (Zhang et al., 2017). Immediately after, mouse MSCs (transduced with

either shControl or shFUT8, and pre-incubated FGF2) were injected intramuscularly (five mice per group), near the fracture site. After 7 days, mice were euthanized and samples fixed and embedded to visualize the injected cells based on tdTomato.

Modeling Analysis

The crystal structure of β_1 integrin was taken from the $\alpha5\beta1$ integrin headpiece in complex with an arginylglycylaspartic acid (RGD) peptide (PDB ID: 3VI4) (Nagae et al., 2012). After minimization and equilibration steps, four independent simulations of 70 ns were collected. To compare glycans with or without core fucose, torsion angles were collected from each simulation with a temporal resolution of 50 ps.

Statistical Analysis

Results were presented as mean ± SEM. Depending on the number of compared conditions, one-way ANOVA, two-way ANOVA, or two-tailed Student's t test were conducted using GraphPad Prism Software; p values < 0.05 were considered statistically significant.

ACCESSION NUMBERS

RNA-seq data are available at GEO under accession number: GEO: GSE115240.

SUPPLEMENTAL INFORMATION

Supplemental Information includes Supplemental Experimental Procedures, four figures, one table, and three videos and can be found with this article online at https://doi.org/10.1016/j.stemcr.2018.06.007.

AUTHOR CONTRIBUTIONS

B.A., D.T., C.S., A.M., A.R., and F.A.F. performed all experiments and analyzed results, with the following exceptions: G.X., D.P., and C.B.L. did the studies related to N-glycan analysis, W.Y. did the studies in mice, L.J. and M.L.A. did the studies in zebrafish, S.K. did the RNA-seq, and A.J. did the *in silico* modeling. F.A.F. and C.B.L. designed the overall project and interpreted results. F.A.F. wrote the manuscript.

ACKNOWLEDGMENTS

We would like to thank Dr. Steven Frese for support in the analysis of RNA-seq data and Lee M. Cheung for technical help on the zebrafish experiments.

Received: November 6, 2017
Revised: June 4, 2018
Accepted: June 6, 2018
Published: July 5, 2018

SUPPORTING CITATIONS

The following references appear in the Supplemental Information: Horwitz et al., 2005; Kirschner et al., 2008; Maier et al., 2015; Sasaki et al., 2013.

REFERENCES

Cummings, R.D., and Pierce, J.M. (2014). The challenge and promise of glycomics. Chem. Biol. *21*, 1–15.

Dalby, M.J., Gadegaard, N., and Oreffo, R.O. (2014). Harnessing nanotopography and integrin-matrix interactions to influence stem cell fate. Nat. Mater. *13*, 558–569.

Fedele, M., Visone, R., De Martino, I., Troncone, G., Palmieri, D., Battista, S., Ciarmiello, A., Pallante, P., Arra, C., Melillo, R.M., et al. (2006). HMGA2 induces pituitary tumorigenesis by enhancing E2F1 activity. Cancer Cell *9*, 459–471.

Federico, A., Forzati, F., Esposito, F., Arra, C., Palma, G., Barbieri, A., Palmieri, D., Fedele, M., Pierantoni, G.M., De Martino, I., et al. (2014). Hmga1/Hmga2 double knock-out mice display a "super-pygmy" phenotype. Biol. Open *3*, 372–378.

Fierro, F.A., Kalomoiris, S., Sondergaard, C.S., and Nolta, J.A. (2011). Effects on proliferation and differentiation of multipotent bone marrow stromal cells engineered to express growth factors for combined cell and gene therapy. Stem Cells *29*, 1727–1737.

Geng, F., Shi, B.Z., Yuan, Y.F., and Wu, X.Z. (2004). The expression of core fucosylated E-cadherin in cancer cells and lung cancer patients: prognostic implications. Cell Res. *14*, 423–433.

Goschnick, M.W., Lau, L.M., Wee, J.L., Liu, Y.S., Hogarth, P.M., Robb, L.M., Hickey, M.J., Wright, M.D., and Jackson, D.E. (2006). Impaired "outside-in" integrin alphaIIbbeta3 signaling and thrombus stability in TSSC6-deficient mice. Blood *108*, 1911–1918.

Grayson, W.L., Bunnell, B.A., Martin, E., Frazier, T., Hung, B.P., and Gimble, J.M. (2015). Stromal cells and stem cells in clinical bone regeneration. Nat. Rev. Endocrinol. *11*, 140–150.

Gronthos, S., Simmons, P.J., Graves, S.E., and Robey, P.G. (2001). Integrin-mediated interactions between human bone marrow stromal precursor cells and the extracellular matrix. Bone *28*, 174–181.

Gu, J., and Taniguchi, N. (2008). Potential of N-glycan in cell adhesion and migration as either a positive or negative regulator. Cell Adh. Migr. *2*, 243–245.

Guo, H.B., Lee, I., Kamar, M., Akiyama, S.K., and Pierce, M. (2002). Aberrant N-glycosylation of beta1 integrin causes reduced alpha5beta1 integrin clustering and stimulates cell migration. Cancer Res. *62*, 6837–6845.

Heino, J., Ignotz, R.A., Hemler, M.E., Crouse, C., and Massague, J. (1989). Regulation of cell adhesion receptors by transforming growth factor-beta. Concomitant regulation of integrins that share a common beta 1 subunit. J. Biol. Chem. *264*, 380–388.

Hong, Q., Lebrilla, C.B., Miyamoto, S., and Ruhaak, L.R. (2013). Absolute quantitation of immunoglobulin G and its glycoforms using multiple reaction monitoring. Anal. Chem. *85*, 8585–8593.

Horwitz, E.M., Le Blanc, K., Dominici, M., Mueller, I., Slaper-Cortenbach, I., Marini, F.C., Deans, R.J., Krause, D.S., and Keating, A.; International Society for Cellular Theraphy (2005). Clarification of the nomenclature for MSC: the International Society for Cellular Therapy position statement. Cytotherapy *7*, 393–395.

Ito, T., Sawada, R., Fujiwara, Y., Seyama, Y., and Tsuchiya, T. (2007). FGF-2 suppresses cellular senescence of human mesenchymal stem

cells by down-regulation of TGF-beta2. Biochem. Biophys. Res. Commun. *359*, 108–114.

Kalomoiris, S., Cicchetto, A.C., Lakatos, K., Nolta, J.A., and Fierro, F.A. (2016). Fibroblast growth factor 2 regulates high mobility group A2 expression in human bone marrow-derived mesenchymal stem cells. J.Cell. Biochem. *117*, 2128–2137.

Karp, J.M., and Leng Teo, G.S. (2009). Mesenchymal stem cell homing: the devil is in the details. Cell Stem Cell *4*, 206–216.

Kirschner, K.N., Yongye, A.B., Tschampel, S.M., Gonzalez-Outeiriño, J., Daniels, C.R., Foley, B.L., and Woods, R.J. (2008). GLYCAM06: a generalizable biomolecular force field. Carbohydrates. J. Comput. Chem. *29*, 622–655.

Kornfeld, R., and Kornfeld, S. (1985). Assembly of asparagine-linked oligosaccharides. Annu. Rev. Biochem. *54*, 631–664.

Maier, J.A., Martinez, C., Kasavajhala, K., Wickstrom, L., Hauser, K.E., and Simmerling, C. (2015). ff14SB: improving the accuracy of protein side chain and backbone parameters from ff99SB. J. Chem. Theor. Comput. *11*, 3696–3713.

Marques, I.J., Weiss, F.U., Vlecken, D.H., Nitsche, C., Bakkers, J., Lagendijk, A.K., Partecke, L.I., Heidecke, C.D., Lerch, M.M., and Bagowski, C.P. (2009). Metastatic behaviour of primary human tumours in a zebrafish xenotransplantation model. BMC Cancer *9*, 128.

Moremen, K.W., Tiemeyer, M., and Nairn, A.V. (2012). Vertebrate protein glycosylation: diversity, synthesis and function. Nat. Rev. Mol. Cell Biol. *13*, 448–462.

Nagae, M., Re, S., Mihara, E., Nogi, T., Sugita, Y., and Takagi, J. (2012). Crystal structure of α5β1 integrin ectodomain: atomic details of the fibronectin receptor. J. Cell Biol. *197*, 131–140.

Park, D., Brune, K.A., Mitra, A., Marusina, A.I., Maverakis, E., and Lebrilla, C.B. (2015). Characteristic changes in cell surface glycosylation accompany intestinal epithelial cell (IEC) differentiation: high mannose structures dominate the cell surface glycome of undifferentiated enterocytes. Mol. Cell. Proteomics *14*, 2910–2921.

Rombouts, W.J., and Ploemacher, R.E. (2003). Primary murine MSC show highly efficient homing to the bone marrow but lose homing ability following culture. Leukemia *17*, 160–170.

Sackstein, R., Merzaban, J.S., Cain, D.W., Dagia, N.M., Spencer, J.A., Lin, C.P., and Wohlgemuth, R. (2008). Ex vivo glycan engineering of CD44 programs human multipotent mesenchymal stromal cell trafficking to bone. Nat. Med. *14*, 181–187.

Sasaki, H., Toda, T., Furukawa, T., Mawatari, Y., Takaesu, R., Shimizu, M., Wada, R., Kato, D., Utsugi, T., Ohtsu, M., et al. (2013). alpha-1,6-Fucosyltransferase (FUT8) inhibits hemoglobin production during differentiation of murine and K562 human erythroleukemia cells. J. Biol. Chem. *288*, 16839–16847.

Schmidt, A., Ladage, D., Schinkothe, T., Klausmann, U., Ulrichs, C., Klinz, F.J., Brixius, K., Arnhold, S., Desai, B., Mehlhorn, U., et al. (2006). Basic fibroblast growth factor controls migration in human mesenchymal stem cells. Stem Cells *24*, 1750–1758.

Solchaga, L.A., Penick, K., Porter, J.D., Goldberg, V.M., Caplan, A.I., and Welter, J.F. (2005). FGF-2 enhances the mitotic and chondrogenic potentials of human adult bone marrow-derived mesenchymal stem cells. J. Cell Physiol. *203*, 398–409.

Taniguchi, N., and Kizuka, Y. (2015). Glycans and cancer: role of N-glycans in cancer biomarker, progression and metastasis, and therapeutics. Adv. Cancer Res. *126*, 11–51.

Trounson, A., and McDonald, C. (2015). Stem cell therapies in clinical trials: progress and challenges. Cell Stem Cell *17*, 11–22.

Tsutsumi, S., Shimazu, A., Miyazaki, K., Pan, H., Koike, C., Yoshida, E., Takagishi, K., and Kato, Y. (2001). Retention of multilineage differentiation potential of mesenchymal cells during proliferation in response to FGF. Biochem. Biophys. Res. Commun. *288*, 413–419.

Wang, X., Chen, J., Li, Q.K., Peskoe, S.B., Zhang, B., Choi, C., Platz, E.A., and Zhang, H. (2014). Overexpression of alpha (1,6) fucosyltransferase associated with aggressive prostate cancer. Glycobiology *24*, 935–944.

Yang, Q., and Wang, L.X. (2016). Mammalian alpha1,6-fucosyltransferase (FUT8) is the sole enzyme responsible for the N-acetylglucosaminyltransferase I-independent core fucosylation of high-mannose N-glycans. J. Biol. Chem. *291*, 11064–11071.

Zhang, H., Kot, A., Lay, Y.E., Fierro, F.A., Chen, H., Lane, N.E., and Yao, W. (2017). Acceleration of fracture healing by overexpression of basic fibroblast growth factor in the mesenchymal stromal cells. Stem Cells Transl. Med. *6*, 1880–1893.

Zhao, Y., Itoh, S., Wang, X., Isaji, T., Miyoshi, E., Kariya, Y., Miyazaki, K., Kawasaki, N., Taniguchi, N., and Gu, J. (2006). Deletion of core fucosylation on alpha3beta1 integrin down-regulates its functions. J. Biol. Chem. *281*, 38343–38350.

Stem Cell Reports, Volume *11*

Supplemental Information

FGF2 Induces Migration of Human Bone Marrow Stromal Cells by Increasing Core Fucosylations on N-Glycans of Integrins

Baarkullah Awan, David Turkov, Cameron Schumacher, Antonio Jacobo, Amber McEnerney, Ashley Ramsey, Gege Xu, Dayoung Park, Stefanos Kalomoiris, Wei Yao, Li-En Jao, Miguel L. Allende, Carlito B. Lebrilla, and Fernando A. Fierro

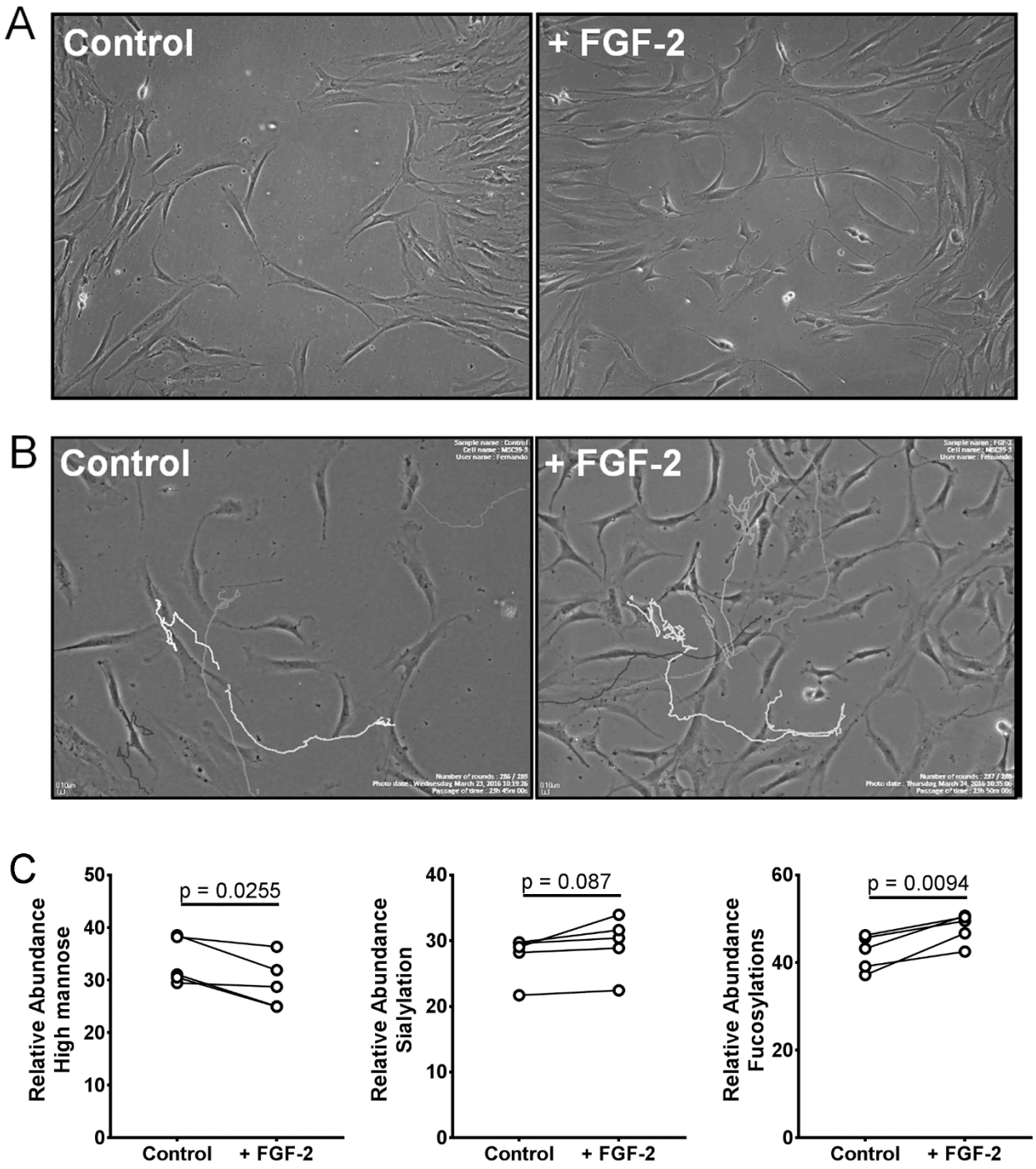

Figure S1. FGF-2 promotes migration and alters N-glycans in MSCs. (A) Wound/scratch assay. MSCs were plated into 24-well plates containing an insert that creates a uniform barrier. Representative images of wound closure. (B) Cell tracking using videomicroscopy. MSCs displacement over time (speed) was recorded and tracked using ImageJ software. Tracks of individual cells are shown as color lines on representative phase contrast images. (C) Changes in high mannose, sialylation and fucosylations in N-glycans of MSCs treated with or without FGF2. Each dot represents MSCs derived from a different donor.

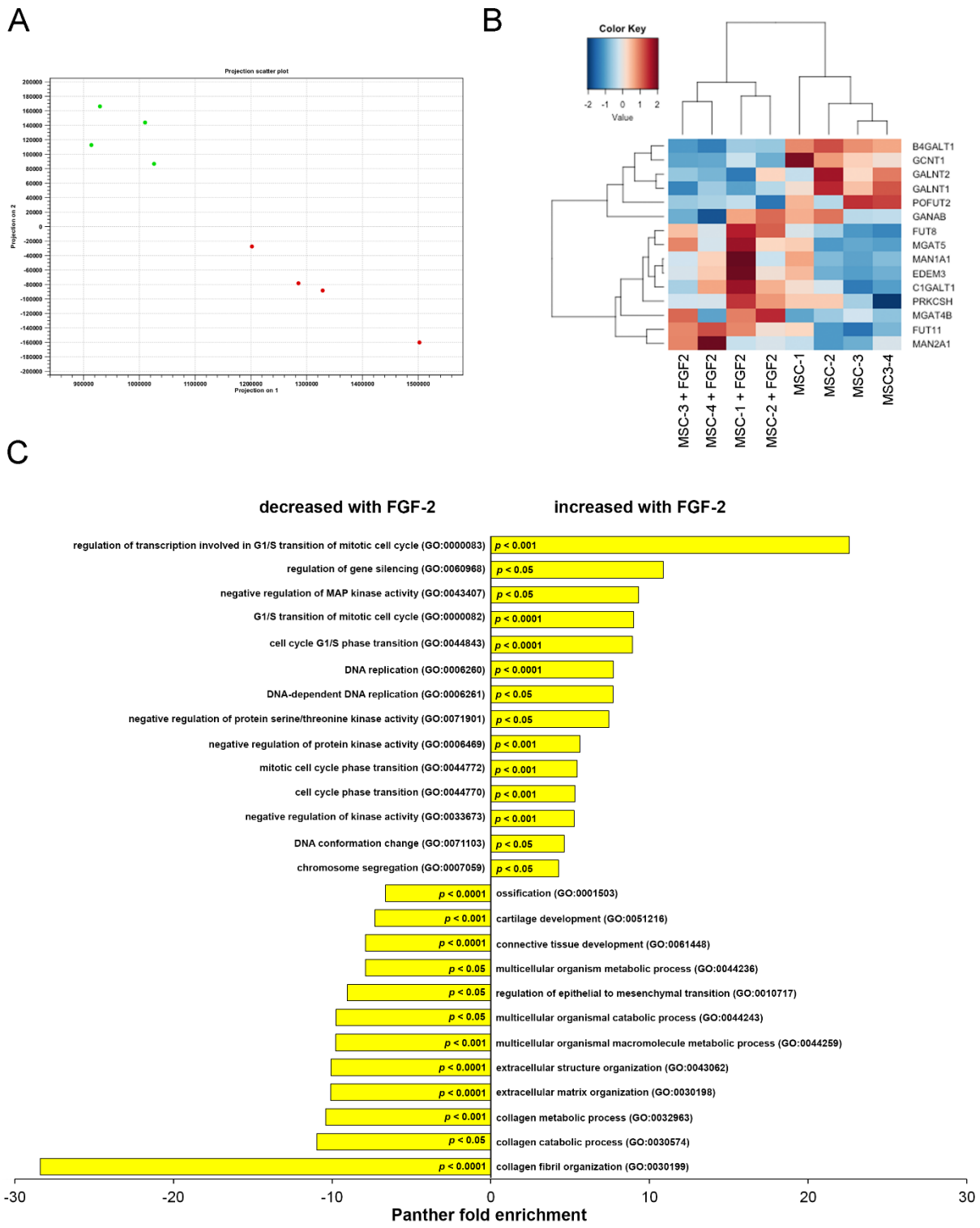

Figure S2. RNAseq of MSC treated with FGF2 (A) Cluster analysis of MSCs treated with (green) or without (red) FGF2. (B) Heat map analysis and hierarchical clustering of differentially expressed genes associated to glycan synthesis. Samples are shown in bottom, where numbers denote MSCs derived from different donors. (C) PANTHER analysis (Mi et al., 2013) of differentially expressed genes, in MSCs treated with FGF2 compared to untreated (control) cells.

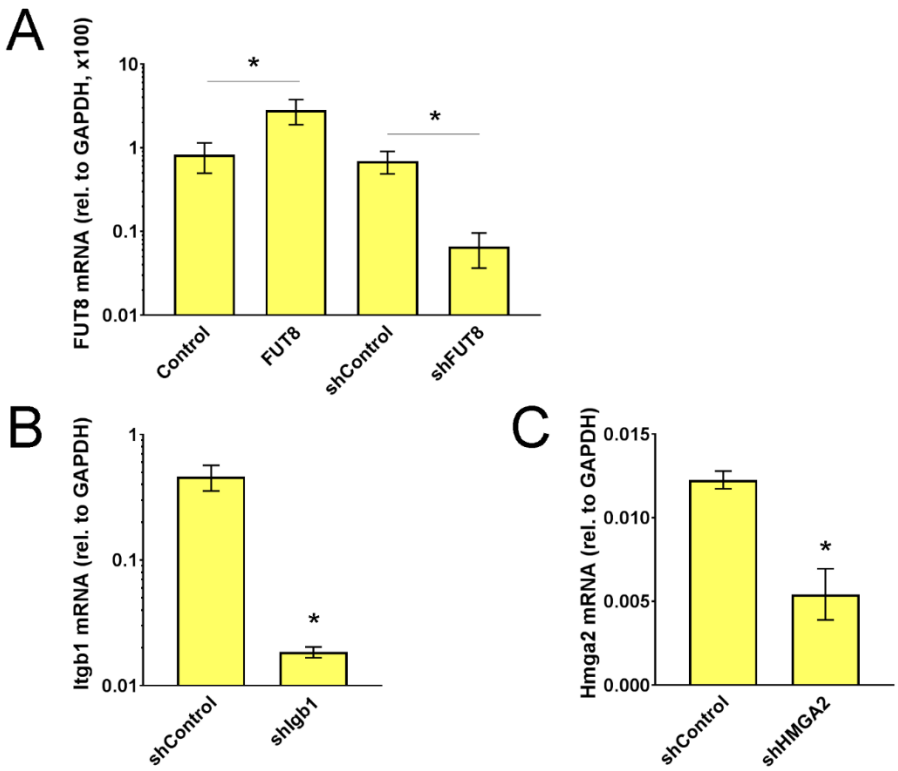

Figure S3. Silencing and over-expression efficiencies using lentivirus. MSCs were transduced with the respective lentiviral vectors. 3 days after, total RNA was extracted and mRNAs measured by real time PCR. (A) N = 6. (B) N = 4. (C) N = 3. * $p < 0.05$ analyzed using a paired Student's *t* test.

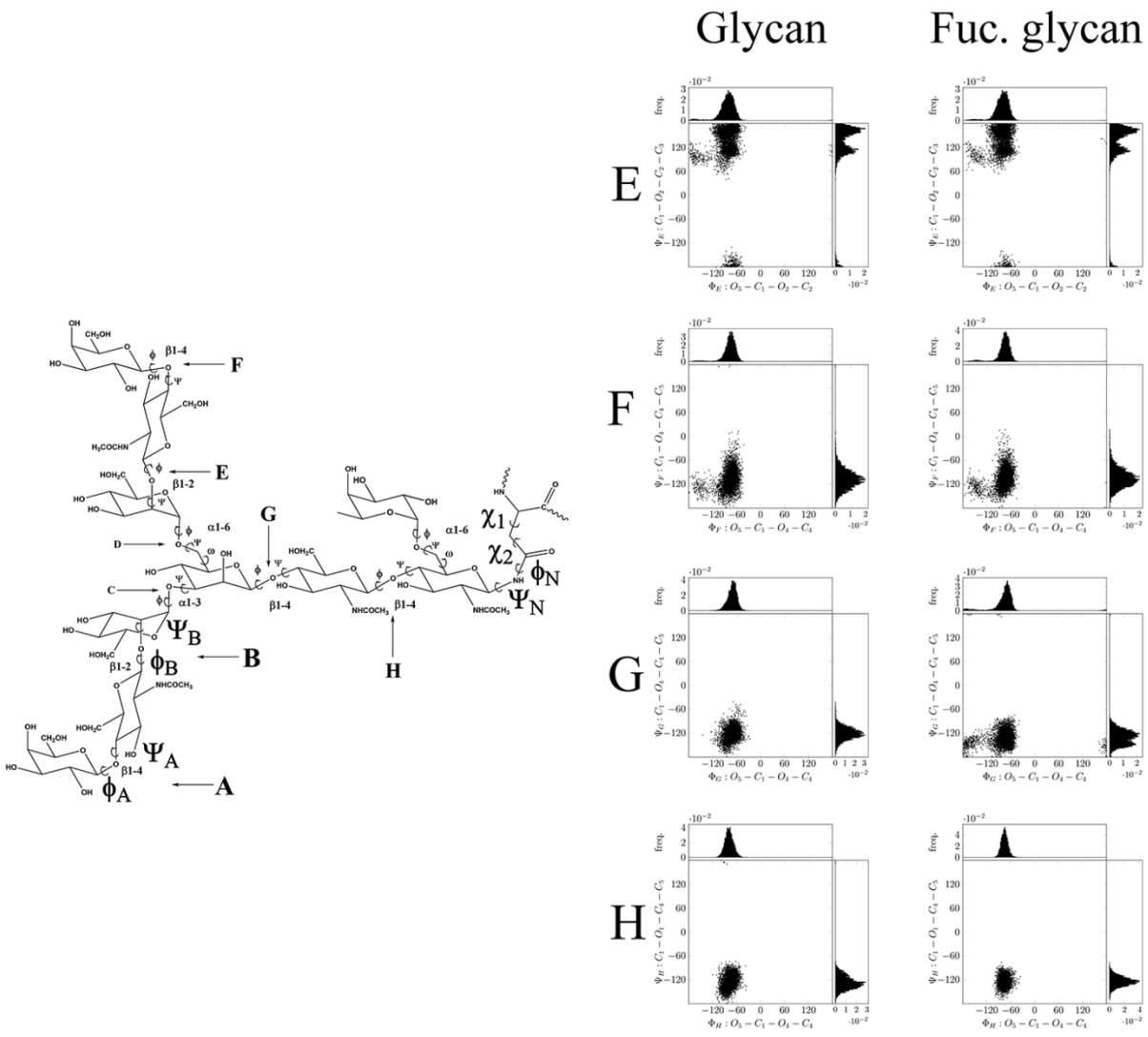

Figure S4. Torsion dihedral angles different to those shown in Figure 4.

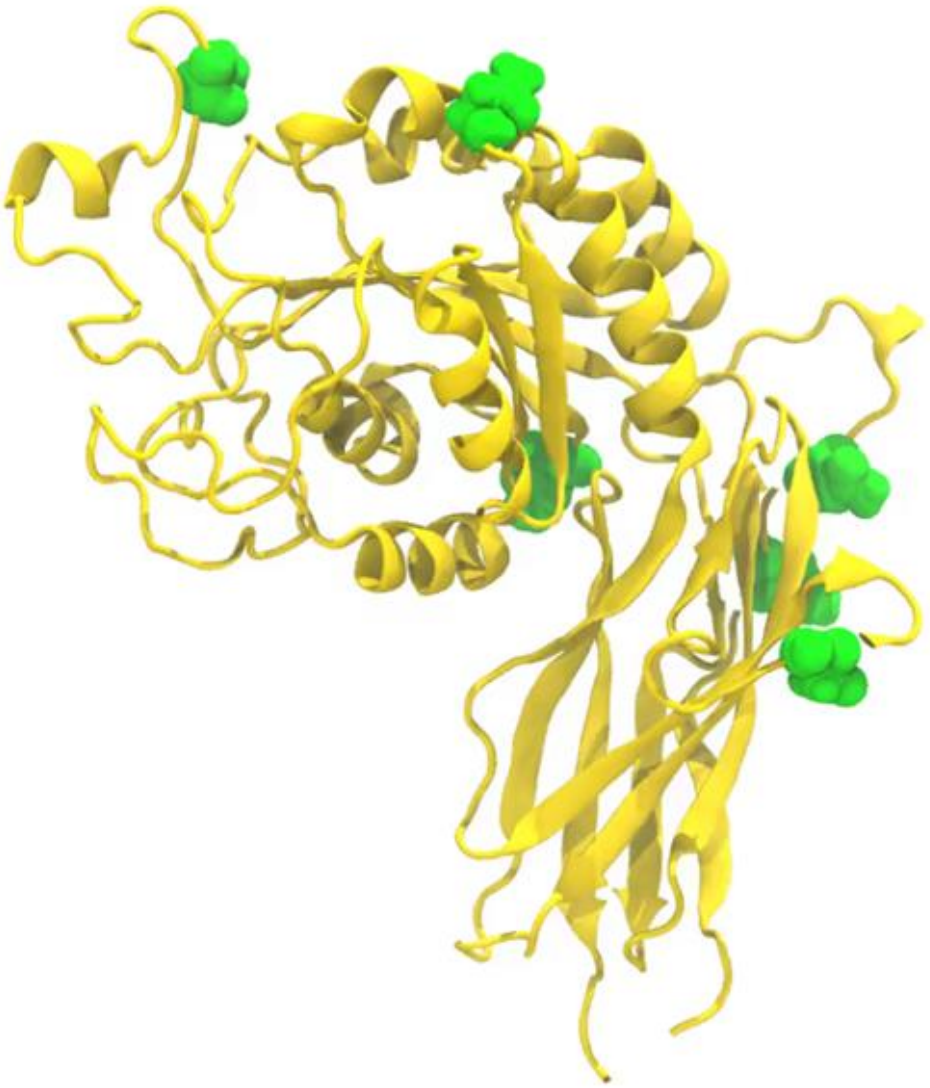

Movie S1 (still image). 3D structure of Integrin β1, with glycosylated residues (green)

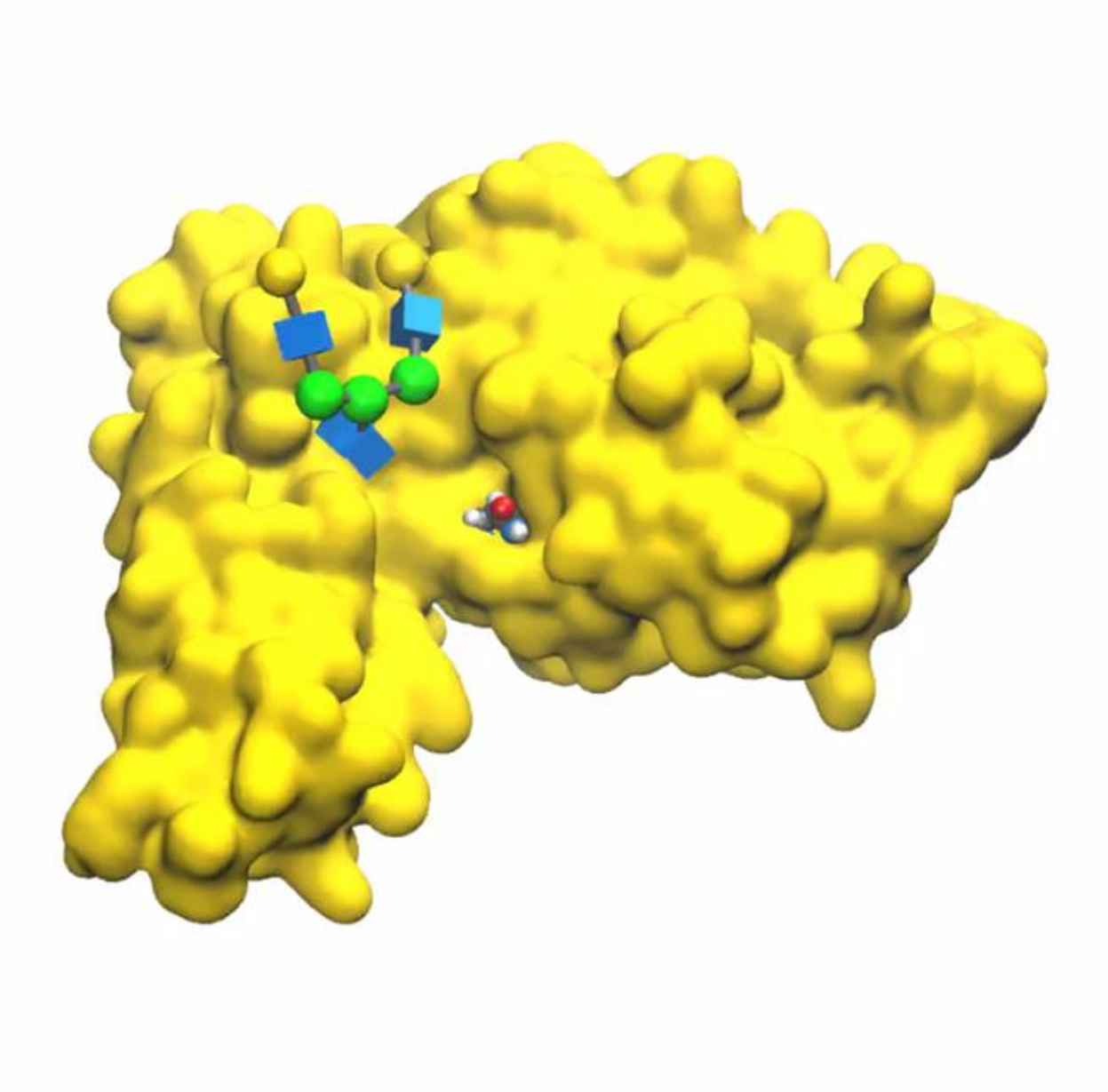

Movie S2 (still image). Simulation of Integrin β_1 with an N-glycan without core-fucosylation. A glycan (see cartoon in Figure 4) was attached to Asn329 *in silico*. This movie shows how that glycan moves freely, with no hydrogen bond with Asn265 (highlighted).

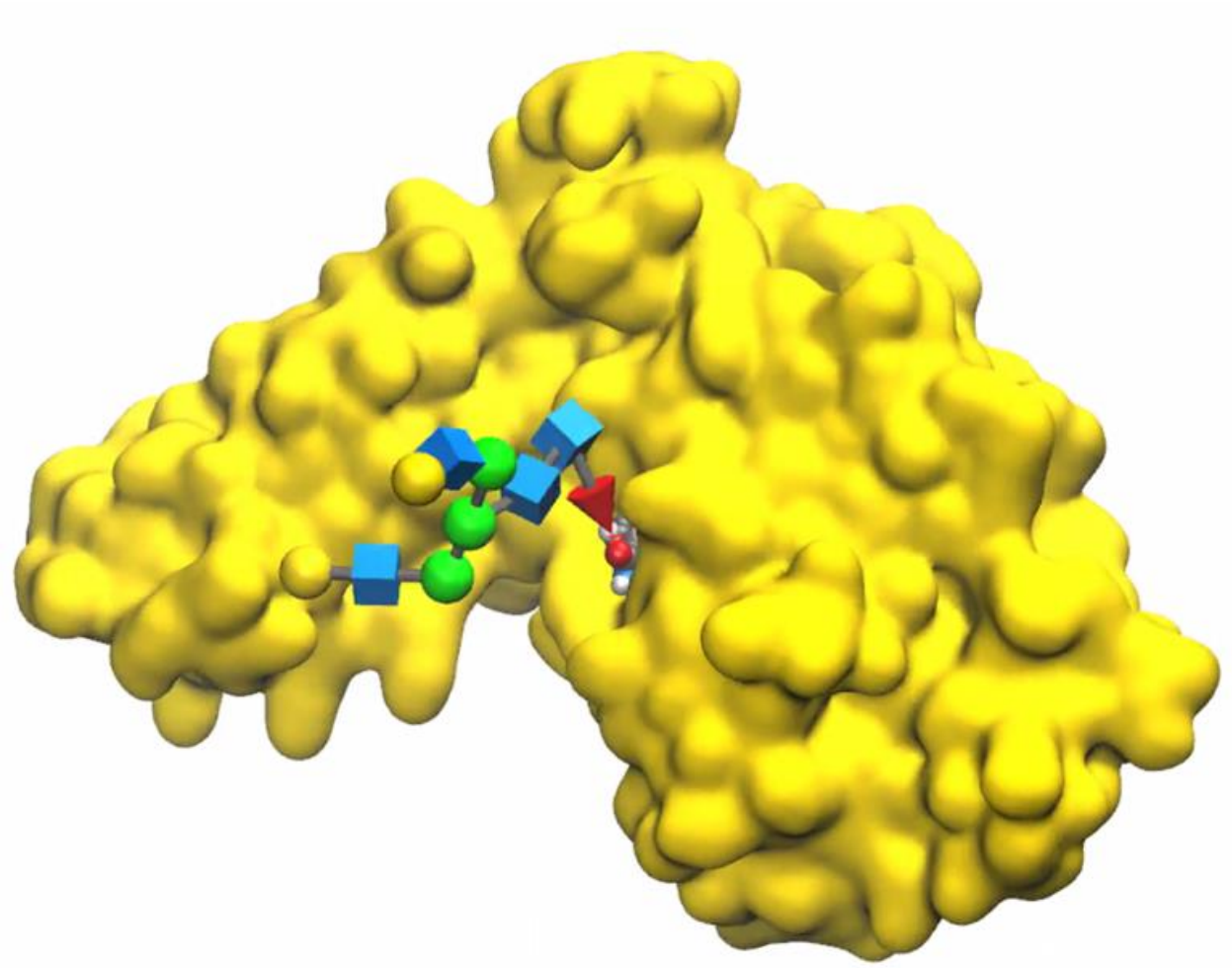

Movie S3 (still image). Simulation of Integrin β_1 with an N-glycan with core-fucosylation. A glycan with core-fucosylation (red cone) was attached to Asn329 *in silico*. This movie shows how that glycan has limited movement, at least partially due to interaction (hydrogen bond) with Asn265 (highlighted).

Supplementary Experimental Procedures

Cell Culture

Mesenchymal Stem Cells (MSCs) were isolated from bone marrow aspirates from healthy donors (Fierro et al., 2011). Fresh bone marrow aspirates (StemExpress) were mixed 1:1 with PBS, layered over Ficoll-Paque PLUS (GE Healthcare) and centrifuged for 30 min at 600 × *g*. Total mononuclear cells were then plated in tissue culture flasks using MEM-alpha (HyClone) supplemented with 10% fetal bovine serum (Atlanta Biologicals) and 1% Penicillin-Streptomycin. After 2 days, non-adherent cells were washed off. Remaining cells were expanded, acquiring the characteristic morphology, immune phenotype and differentiation potential of MSCs (Horwitz et al., 2005). To isolate mouse MSCs, two months old, male 129vJ mice were humanely euthanized. Bone marrows from both femurs and tibiae, were flushed using cell culture media, and directly plated into 6-well plates. After 2 days adherent cells were washed off and for the next two passages, Trypsin treatment was limited to 4 minutes, to purify MSC from other adherent cells. All experiments were performed with MSCs in passage 2 - 6, where each passage represents 3-4 population doublings (5-7 days in culture). Each experiment repetition (N) was performed with MSCs derived from a different donor. All experiments with FGF2 use 24 hours incubation, 10ng/ml FGF2.

Wound/scratch assay

MSCs were seeded into 24-well plates with Cytoselect inserts (Cell Biolabs), at 25,000 cells per side (6 replicates per condition). The next day, inserts were removed and media was changed. Pictures were taken immediately and 24 hours after, unless otherwise described. Wound area was quantified using TScratch software (Geback et al., 2009). For experiments with engineered cells, transductions were performed 3 days prior to the assay. For experiments with FGF2, supplementation was started at the moment of seeding the cells (24 hours prior to removing the inserts). For experiments with extracellular matrix, coating was performed for 1 hour at 37C, followed by two washes with PBS, prior to seeding the cells. For collagen (type I, from rat tail, Sigma-Aldrich), Fibronectin (from human plasma, Gibco), Laminin (Sigma-Aldrich), the final concentrations were all 10μg/ml.

Videomicroscopy

MSCs were plated in 35mm petri-dishes (20,000 cells/dish) and placed in a BioStation microscope (Nikon) for videomicroscopy, while maintaining the cells at 37˚C and 5% CO_2. During recording, each dish was photographed in 6-9 fields of view over 24 hours (unless otherwise

stated). Movies were then analyzed using ImageJ software to determine individual cell displacement over time (speed). For experiments with extracellular matrix, coating was performed as described for the wound/scratch assays, but in 35mm petri-dishes.

RNA-seq

Total RNA from four different donors treated with or without FGF2 (One million cells per sample) was extracted using a Direct-zol RNA Mini-Prep kit (Zymo Research), following manufacturer's instructions. Total RNA was then submitted to Beijing Genomics Institute (BGI) at UC Davis. Here, RNA quality was determined using Agilent 2100. For all samples, RNA integrity number was above 8.0. cDNA library from total mRNA was built using an Illumina kit. Sequencing was performed in two SE50 lanes using the Hiseq2000 platform (Illumina). Average number of reads per sample was 20.7 x 10^6. Results were analyzed, normalized and semi-quantified using DESeq2 software (Love et al., 2014).

Real time PCR

RNA extraction was performed using a Direct-zol RNA Mini-Prep kit (Zymo Research), following manufacturer's instructions. Real time PCR were performed using Taqman gene expression assays (Applied Biosystems) and Taqman Universal Master Mix reagents (Applied Biosystems). The sequences are undisclosed by the manufacturer, but are identified by the following Assay ID: FUT8: Hs00189535_m1, FUCA1: Hs00609173_m1, HMGA1: Hs00852949_g1*, HMGA2: Hs04397751_m1, E2F1: Hs00153451_m1, FGFR2: Hs01552918_m1, DOCK4: Hs00206807_m1, PODXL: Hs01574644_m1, ITGA3: Hs01076879_m1, RHOB: Hs05051455_s1*, ITGA11: Hs01012939_m1, ITGAV: Hs00233808_m1, ITGB1: Hs01127536_m1, GAPDH: Hs02786624_g1. For all assays, the probe spans exons, except for those with asterisk (*), where both primers and probe map within a single exon.

NanoLC/ESI-QTOF-MS

One million MSCs treated with or without FGF2; derived from five different donors, where lifted with Trypsin, washed with PBS and resuspended in homogenization buffer (0.25 M sucrose, 20 mM HEPES-KOH (pH 7.4), and 1:100 protease inhibitor mixture (EMD Milipore)). Cells were lysed on ice using a probe sonicator (Qsonica) and lysates were pelleted by centrifugation at 2000 × *g* for 10 min to remove the nuclear fraction and unlysed cells followed by a series of ultracentrifugation steps at 200,000 × *g* for 45 min to remove other nonmembrane subcellular

fractions (Park et al., 2015). Membrane pellets were then suspended with 100 μl of 100 mM NH_4HCO_3 in 5 mM dithiothreitol and heated for 10 s at 100 °C to thermally denature the proteins. To release the glycans, 2 μl of peptide N-glycosidase F (New England Biolabs) was added to the samples, which were then incubated at 37 °C in a microwave reactor (CEM Corporation) for 10 min at 20 watts. After addition of 400 μl of ice-cold ethanol, samples were frozen for 1 h at -80 °C to precipitate deglycosylated proteins and centrifuged for 20 min at 21,130 × *g*. The supernatant containing N-glycans was collected and dried.

Released N-glycans were purified by solid-phased extraction using porous graphitized carbon packed cartridges (Grace, Deerfield, IL). Cartridges were first equilibrated with alternating washes of nanopure water and a solution of 80% (v/v) acetonitrile and 0.05% (v/v) trifluoroacetic acid in water. Samples were loaded onto the cartridge and washed with nanopure water at a flow rate of 1 ml/min to remove salts and buffer. N-Glycans were eluted with a solution of 40% (v/v) acetonitrile and 0.05% (v/v) trifluoroacetic acid in water and dried. Analysis was performed as previously described (Park et al., 2015).

Lentiviral constructs and transduction

To silence FUT8, an shRNA was designed based on a previously published target site (Sasaki et al., 2013). This was then cloned into the lentiviral construct pCCLc-U6-shRNA-PGK-dTomato, where shRNA is either a non-targeting sequence (Control) or the shRNA targeting FUT8. To silence HMGA2, the previously published lentivirus shHMGA2-2 (Kalomoiris et al., 2016) was used. Overexpression of FUT8 was performed by cloning the protein coding sequence of FUT8 (1,728bp) into the lentiviral construct pCCLc-MNDU3-X-PGK-EGFP-WPRE, where X is either no sequence (control) or FUT8. All transductions were performed using protamine sulfate (20μg/ml) and with sufficient lentivirus to generate 90–95% GFP/dTomato positive MSCs, 3 days after transduction.

Western Blot

Transduced MSCs, treated with or without FGF2 were lysed for protein extraction using RIPA Buffer (Thermo Scientific) with 1% Halt Proteinase and Phosphatase Inhibitor Cocktail (Thermo Scientific). Proteins were extracted by strong agitation for 20 min at 4˚C, then centrifuged at 12,000g for 10 min and stored at -80°C. For western blots, 30μg of proteins were loaded into 10% polyacrylamide gels and transferred into polyvinylidene fluoride membranes (BioRad). Blots were then incubated with anti-FUT8 polyclonal antibody (250ng/ml, RnD Systems) overnight. After

protein detection, both membranes were stripped and incubated with anti-actin (200ng/ml, clone AC15, Sigma-Aldrich).

LC-MS/MS analysis of glycopeptides

Membrane proteins were dissolved in 8 M urea, denatured at 55°C with 18 mM dithiothreitol, and alkylated with 27 mM iodoacetamide in dark at room temperature. The mixture was then diluted to 1 M urea with 50 mM ammonium bicarbonate, and incubated with 1 µg trypsin at 37°C overnight. Solid-phased extraction using iSPE-HILIC cartridges (Nest Group, MA) was performed to enrich the glycopeptides. Cartridges were conditioned with alternating washes of 0.1% (v/v) trifluoroacetic acid in water, and 80% (v/v) acetonitrile with 1% (v/v) trifluoroacetic acid in water. Peptides were loaded onto the column, and washed with 1% (v/v) trifluoroacetic acid and 80% (v/v) acetonitrile in water. Enriched glycopeptides were eluted with a solution of 0.1% (v/v) trifluoroacetic acid in water and dried. Analysis of the enriched glycopeptides was performed on a Q Exactive Plus mass spectrometer (Thermo Scientific, CA). Glycopeptide identification was performed using Byonic software (Protein Metrics Inc.).

Migration assay of MSCs in zebrafish

Wild type zebrafish embryos of the NHGRI-1 (LaFave et al., 2014) strain were collected shortly after fertilization and allowed to develop until the mid blastula stage (3-4 hpf). Embryos were dechorionated manually and mounted on an agarose mold for transplantations. MSCs were loaded into a borosilicate pulled Pasteur pipette and were transferred into zebrafish embryos by mild pressure using a mouth piece and latex tubing or a custom-made Hamilton syringe; 20 to 50 MSCs were introduced into each embryo. Embryos were incubated at 28.5˚C for one day before imaging and scoring the position of the transplanted cells under fluorescent illumination. Images were captured on a Leica M165 FC dissecting scope equipped with a Leica DFC7000 T camera.

Migration assay toward bone fracture in mice

Closed transverse diaphysis fractures of the right femur were generated in ten 2-month-old mice using as previously described [Zhang et al 2017]. Briefly, fractures were created at the mid-femur using a drop-weight blunt guillotine device. Immediately after, mouse MSC (transduced with either shControl or shFUT8, and pre-incubated for 24 hours with 10ng/ml FGF2) were injected intramuscularly (5 mice per group; 10^5 cells per mouse), near the site of fracture and on the opposite (left, unfractured) thigh. After 7 days, mice were euthanized and samples embedded

in optimum cutting temperature (OCT) for cryosections. Injected cells were directly visualized based on tdTomato expression and DAPI staining for total nuclei.

Modelling System Composition, Minimization, Equilibration, and Production

The crystal structure of β_1 integrin was taken from the α5β1 integrin headpiece in complex with an RGD peptide (PDB ID: 3VI4) (Nagae et al., 2012). Chain D, one of the β_1 integrins, was selected and truncated to Asn_{78} and Cys_{460}. To prevent addition of charges, the ends were capped with either an acetyl or amide group at the N-terminus and C-terminus, respectively. First, the non-glycosylated structure was used as control, while two other structures with a glycan and a core fucosylated glycan in Asn_{265}, were also built. The glycans structures (DGalb1-4DGlcpNAcb1-2DManpa1-3[DGalb1-4DGlcpNAcb1-2DManpa1-6]DManpb1-4DGlcpNAcb1-4DGlcpNAcb1-OH, and DGalb1-4DGlcpNAcb1-2DManpa1-3[DGalb1-4DGlcpNAcb1-2DManpa1-6]DManpb1-4DGlcpNAcb1-4[LFucpa1-6]DGlcpNAcb1-OH) were built using Glycam (Kirschner et al., 2008a). The primary hydroxyl groups of DGlcpNAcb1-OH were deleted for each glycan and then docked near the glycosylation site with UCSF Chimera (Pettersen et al., 2004). Each system was composed using AmberTools16 packages (Case DA, 2017), and simulated with Amber16's GPU accelerated PMEMD (Salomon-Ferrer et al., 2013).

Each structure was loaded into tLeap using the protein ff14SB (Maier et al., 2015) for the protein and GLYCAM 06j-1 for carbohydrates (Kirschner et al., 2008b). Using tLeap, disulfide bonds for β1 integrin, the covalent bond between the Asn_{265} amide group and the glycans, and monosaccharide bonds in the glycans were made. Each structure was then solvated with a rectangular box with at least 10 Å of TIP3P water layer around. Two sodium ions were then added to neutralize each system. The ending size of each system was 57,469 atoms (control), 70,528 atoms for glycosylated β_1), and 63,459 atoms for β_1 with core fucosylated glycan.

Structures were then minimized using a two-step method. In the first minimization of 100,000 cycles, a 1 kcal/mol−Å restrain was placed on the glycans, and proteins, excluding their hydrogens. During the second step, the restrain was removed and the systems were further minimized for another 200,000 steps. The systems were then equilibrated at constant volume and temperature, and gradually warmed to 300˚K over 500 ps with a 2-fs time step and with the Langevin Thermostat—this time step and thermostat with a collision frequency of 2 was used hereafter. Once at 300˚K, the systems were maintained for an additional 500ps. After equilibration, four independent simulations of 70 ns with constant temperature (300˚K), and constant pressure (1 atm)—maintained by the Berendsen Thermostat—were collected.

Modelling Analysis

All trajectory analysis was conducted with CPPTRAJ (Roe and Cheatham, 2013). The root means square deviation (RMSD) between the alpha carbons in β_1 was calculated relative to the minimized structure. During simulation, trajectories converged after 10 ns for β_1 with glycan and 20-30 ns for β_1 with core fucosylated glycan. Although, RSMD were different, both equilibrated for each structure. Trajectory analysis for the core fucosylated glycan with integrin was conducted for both times yielding the same results. To compare glycans with or without core fucose, torsion angles were collected from each simulation with a temporal resolution of 50 ps. The torsion angles were defined as Φ: O_5-C_1-O_1-C'_X, Ψ psi: C_1-O_1-C'_X-C'_{X+1}, ω: O_1-C'_6-C'_5-O'_5, χ_1: N–C_α–C_β–C_γ, χ_2: C_α–C_β–C_γ–N; Ψ_N: C_β–C_γ–N–C_1; Φ_N: C_γ–N–C_1–O_5. The torsion angles are plotted in double distribution plots to better understand the flexibility of each glyosidic linkage.

The trajectory for each simulation was visualized with Visual Molecular Dynamics (VMD) (Humphrey et al., 1996). To better represent each structure, Tachyon ambient occlusion lighting and 3D-symbol nomenclature (Varki et al., 2015) for glycans was used. The trajectory for β_1 was smoothed with a windows size of 4, while the glycan trajectory was not modified. This allowed the representation of the full motion of the glycan while reducing fluctuations in β_1.

Statistical analysis

Results were presented as mean ± SEM. Depending on the number of compared conditions, 1-way ANOVA, 2-way ANOVA or two tailed Student's t-test were conducted using Graph-Pad Prism Software. P values <0.05 were considered statistically significant.

Acknowledgements

We would like to thank Dr. Dr. Steven Frese for support in the analysis of RNAseq data and Lee M. Cheung for technical help on the zebrafish experiments.

Supplementary References

Case DA, C.D., Cheatham TE, et al. (2017). AMBER 2017, University of California, San Francisco.

Geback, T., Schulz, M.M., Koumoutsakos, P., and Detmar, M. (2009). TScratch: a novel and simple software tool for automated analysis of monolayer wound healing assays. BioTechniques *46*, 265-274.

Humphrey, W., Dalke, A., and Schulten, K. (1996). VMD: Visual molecular dynamics. Journal of Molecular Graphics *14*, 33-38.

LaFave, M.C., Varshney, G.K., Vemulapalli, M., Mullikin, J.C., and Burgess, S.M. (2014). A defined zebrafish line for high-throughput genetics and genomics: NHGRI-1. Genetics *198*, 167-170.

Love, M.I., Huber, W., and Anders, S. (2014). Moderated estimation of fold change and dispersion for RNA-seq data with DESeq2. Genome biology *15*, 550.

Pettersen, E.F., Goddard, T.D., Huang, C.C., Couch, G.S., Greenblatt, D.M., Meng, E.C., and Ferrin, T.E. (2004). UCSF Chimera—A visualization system for exploratory research and analysis. Journal of Computational Chemistry *25*, 1605-1612.

Mi, H., Muruganujan, A., Casagrande, J.T., and Thomas, P.D. (2013). Large-scale gene function analysis with the PANTHER classification system. Nature Protocols *8*, 1551-1566.

Roe, D.R., and Cheatham, T.E. (2013). PTRAJ and CPPTRAJ: Software for Processing and Analysis of Molecular Dynamics Trajectory Data. Journal of Chemical Theory and Computation *9*, 3084-3095.

Salomon-Ferrer, R., Götz, A.W., Poole, D., Le Grand, S., and Walker, R.C. (2013). Routine Microsecond Molecular Dynamics Simulations with AMBER on GPUs. 2. Explicit Solvent Particle Mesh Ewald. Journal of Chemical Theory and Computation *9*, 3878-3888.

Varki, A., Cummings, R.D., Aebi, M., Packer, N.H., Seeberger, P.H., Esko, J.D., Stanley, P., Hart, G., Darvill, A., Kinoshita, T.*, et al.* (2015). Symbol Nomenclature for Graphical Representations of Glycans. Glycobiology *25*, 1323-1324.